

P-2

**BONE GEOMETRY, STRUCTURE, AND MINERAL DISTRIBUTION USING DUAL ENERGY X-RAY ABSORPTIOMETRY (DXA)**

Robert Whalen and Tammy Cleek

NASA/Ames Research Center  
Moffett Field, CA USA 94035

**INTRODUCTION**

Dual energy x-ray absorptiometry (DXA) is currently the most widely used method of analyzing regional and whole body changes in bone mineral content (BMC) and areal ( $g/cm^2$ ) bone mineral density (BMD). However, BMC and BMD do not provide direct measures of long bone geometry, structure, or strength, nor do regional measurements detect localized changes in *other* regions of the same bone.

The capabilities of DXA can be enhanced significantly by special processing of pixel BMC data which yields cross-sectional geometric and structural information [1,2]. We have extended this method of analysis in order to develop non-uniform structural beam models of long bones.

**METHODS**

*Theory*

Cross-sectional area, area centroid, and the moment of inertia in the plane of the x-ray beam can be computed by integrating pixel BMC across the scan width. The discretized equations for materials of uniform density are

Cross-sectional area,  $A_t$ :  $A_t = \sum t_i \Delta x$

Centroid,  $x^*$ :  $x^* = (1/A_t) \sum x_i t_i \Delta x$

Moment of inertia,  $I^*_y$ :  $I^*_y = \sum (x_i - x^*)^2 t_i \Delta x$

In these equations the summation is over the phantom (or bone) width,  $t_i$  is the phantom or bone mineral thickness at the  $i$ th pixel obtained from attenuation data, and  $\Delta x$  is the pixel spacing (width).

To obtain principal moments and orientation of the principal axes at each scan cross-section, the complete inertia matrix is first determined from independent analyses of 3 non-coplanar scans (0, 45, 90 degrees in our analysis here), followed by diagonalization of the inertia matrix [3,4]. The diagonal elements are the principal maximum and minimum moments of inertia. Components of the transformation matrix are direction cosines of the principal axes. Axes are orthogonal to each other.

Structural beam models are generated by combining the section properties from each cross-section.

Note: In this preliminary study cadaver scans were not calibrated to bone tissue and no correction was made for bone porosity. Calculated values are proportional, but not equal, to moments of inertia of the bone mineral attenuating the beam.

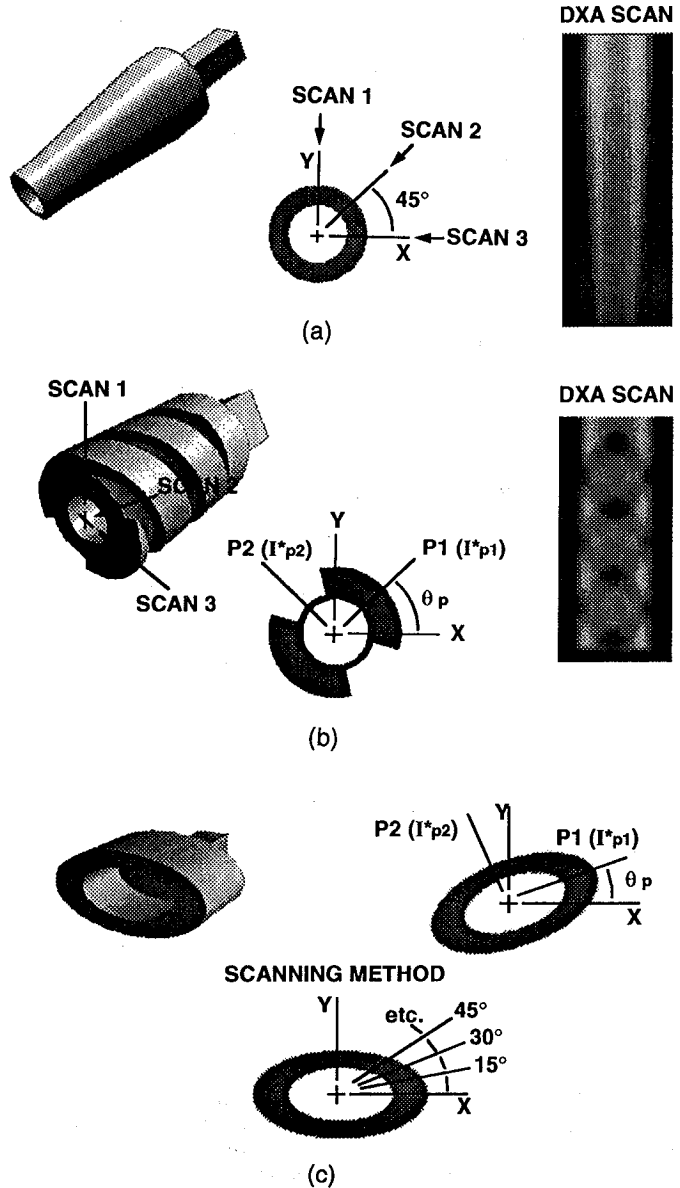
*Beam calibration*

All scans were taken with the spine scan mode of Hologic's QDR-1000W bone densitometer. Areal resolution is  $\sim 1.0 mm^2$  with a line spacing of 1.0 mm and pixel width of  $\sim 1.0 mm$ . An aluminum step phantom of twenty 0.050 inch increments was scanned to obtain calibration regression equations for the air, bone, and tissue segments of Hologic's internal calibration wheel. Regression equations were then used to convert beam attenuation data to equivalent thicknesses of aluminum. Only the high energy beam was used since all scans were done in air.

*Phantom designs*

Aluminum phantoms were designed and machined to investigate the influence of different phantom shapes and angular positions on the accuracy of computed section properties (Figures 1a-c). An entire cadaver femur was also scanned and analyzed.

True or "expected" values were computed from micrometer measurements of the aluminum phantoms or were set by the machining operation (eg., helical pitch angle).



Figures 1. Aluminum (bone equivalent) phantoms with scan directions. a). tapered tube, b) double lead helix, and c) elliptical tube. P1, P2, I\*p1, and I\*p2 represent principal axes and moments of inertia.

### Scanning procedure

The scan direction was perpendicular to the long axis of the phantoms and femur. Objects were scanned along their entire length, then rotated axially with an indexer and scanned completely again. The tapered tube, helix, and cadaver femur were scanned in 3 non-coplanar planes of 0, 45, and 90 degrees (see Figures 1a,b). The elliptical tube (Figure 1c) was scanned 12 times in 15 degree increments (0 to 165 degrees).

### Analysis

Computer programs accessed raw attenuation data, converted attenuation data to equivalent thicknesses, and computed section properties from single and multiple, non-coplanar scans.

## RESULTS

### Externally tapered tube:

Cross-sectional areas and moments of inertia (Figure 2) computed over the length of the tube were within 2% and 4%, respectively, of their expected values and independent of phantom width and wall thickness. (Circular cross-sections have equal principal moments of inertia and no preferred orientation.)

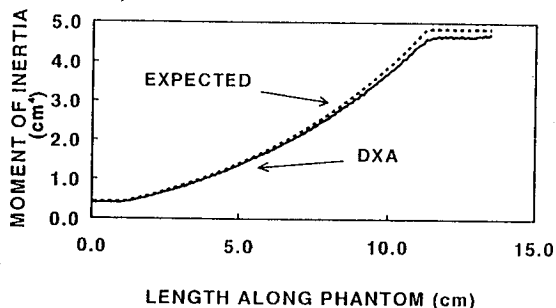


Figure 2. Tapered tube: calculated and "true" moment of inertia.

### Double lead helix:

Orientation of the principal major axis along the phantom was estimated from the 3 non-coplanar scans with virtually no error (Figure 3). Calculated principal moments of inertia,  $I_{max}$  and  $I_{min}$ , were constant as expected.

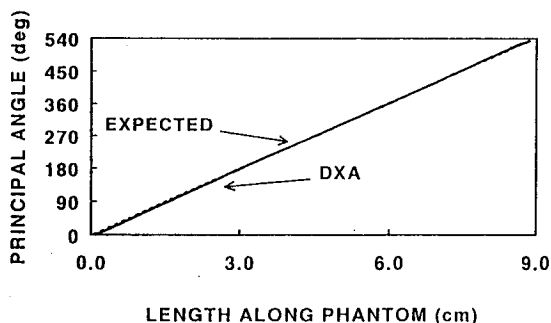


Figure 3. Double lead helix: predicted principal axis orientation.

### Elliptical tube:

Section properties were insensitive to phantom angular position. Initial orientations of the phantom investigated were 0, 15, 30, 45, 60, 75, and 90 degrees. The 3 non-coplanar planes used in each analysis were then taken at 0, 45, and 90 degrees to the initial position, eg., initial position of 15 degrees and scan 1, scan 2, and scan 3 directions of 15, 60, 105 degrees. Principal major axis orientation was uniformly underestimated by ~ 1 degree indicating a probable initial positioning error. Principal moments of inertia were low by ~ 7-8% (Figure 4).

### Cadaver femur:

As expected the principal moments of inertia (see above note) are larger at the proximal and distal ends with the major axis oriented in the medial/lateral plane (Figure 5). The principal major axis rotates 90 degrees to the anterior/posterior plane in the mid-diaphysis, although the bone cross-section is nearly isotropic in this region since  $I_{max}$  and  $I_{min}$  are nearly equal to each other.

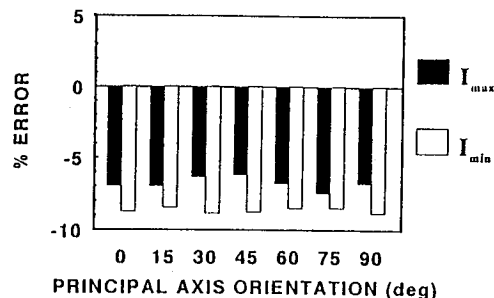


Figure 4. Elliptical tube: Influence of phantom orientation on the principal moments of inertia.

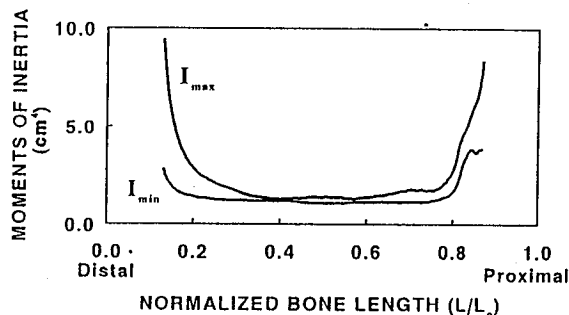


Figure 5. Femur: principal "moments of inertia" along the femur.

## DISCUSSION

Our initial efforts have concentrated on validating our approach and algorithms using phantoms of known material properties and geometries. Good agreement was found between experimentally determined and "true" section properties of axi- and non-axisymmetric phantoms. Errors were introduced in regions of high density (thickness) gradients. These errors could be reduced with a different scanning method.

It is important to note that the errors are not due to noise which is very small (see Figures). Therefore, precision of repeated measurements will be higher. For example, although estimates of  $I_{max}$  and  $I_{min}$  for the elliptical section were 7-8% low, they were within 1-2% of each other (see Figure 4).

Whether a single scan or multiple scans are used, we believe this method of analysis will provide a useful link between changes in local loss and re-organization of bone mineral and changes in long bone strength which occurs with changes in daily activity patterns, space flight, and spinal cord injury.

## REFERENCES

1. Martin and Burr (1984) *J Biomech*, 17: 195-201.
2. Beck et al. (1990) *Invest Radiol*, 25: 6-18.
3. Strength of Materials, S. Timoshenko, 1976.
4. Matrix Analysis for Engineers, J. Gere and W. Weaver; D. Van Nostrand Co., 1965.